
Clarity: The Flexibility-Interpretability Trade-Off in Sparsity-aware Concept Bottleneck Models

Konstantinos P. Panousis¹ Diego Marcos²

Abstract

The widespread adoption of Vision-Language Models (VLMs) across fields has amplified concerns about model interpretability. Distressingly, these models are often treated as black-boxes, with limited or non-existent investigation of their decision making process. Despite numerous post- and ante-hoc interpretability methods, systematic and objective evaluation of the learned representations remains limited, particularly for sparsity-aware methods that are increasingly considered to “induce interpretability”. In this work, we focus on Concept Bottleneck Models and investigate how different modeling decisions affect the emerging representations. We introduce the notion of *clarity*, a measure, capturing the interplay between the downstream performance and the sparsity and precision of the concept representation, while proposing an interpretability assessment framework using datasets with ground truth concept annotations. We consider both VLM- and attribute predictor-based CBMs, and three different sparsity-inducing strategies: per example ℓ_1 , ℓ_0 and Bernoulli-based formulations. Our experiments reveal a critical trade-off between flexibility and interpretability, under which a given method can exhibit markedly different behaviors even at comparable performance levels. The code will be made publicly available upon publication.

1. Introduction

The recent advent of Vision-Language Models (VLMs) has driven an unprecedented adoption of modern deep architectures in a variety of applications and domains. Unfortunately, these models are frequently treated like black-boxes;

¹Department of Statistics, Athens University of Economics and Business, Athens, Greece ²UMR TETIS, Inria, EVERGREEN, Univ Montpellier, Montpellier, France. Correspondence to: Konstantinos P. Panousis <panousis@aub.gr>, Diego Marcos <diego.marcos@inria.fr>.

Preprint. January 30, 2026.

they map inputs to outputs with little to no systematic analysis of their decision making process. This lack of transparency raises serious questions about their confident deployment in critical settings, further amplifying the need for transparent and interpretable architectures.

Concept Bottleneck Models (CBMs) (Koh et al., 2020), and concept-based models in general, aim at tackling this problem; these constitute ante-hoc methods, where the aim is to create inherently interpretable models by constructing a *bottleneck*, i.e., a human interpretable layer that is used to generate the final prediction towards the downstream task. CBMs were initially considered using hand-annotated concepts, which are labor intensive and costly or even unfeasible to produce; at the same time, their dependence on a restricted set of concepts led to significant performance degradation. To bypass this limitation, recent works leveraged VLMs, enabling the use of unrestricted concept sets either hand-crafted, automatically extracted or even machine generated via LLMs (Yang et al., 2023; Oikarinen et al., 2023). While this shift paved the way for unrestricted concept sets that are shown to be quite effective for task performance (Oikarinen et al., 2023), it came at the expense of interpretability. Indeed, VLM-based approaches typically consider thousands of concepts, rendering the investigation of the bottleneck a challenging and unintuitive task, while other issues were further intensified, such as information leakage (Margelou et al., 2021; Schoen et al., 2025).

Sparsity-aware methods aim at solving this issue (Yang et al., 2023; Oikarinen et al., 2023; Panousis et al., 2023). However, these often fail to properly assess the actual impact on model interpretability, instead emphasizing metrics such as classification performance and overall sparsity, typically complemented by qualitative visualizations of the learned representations. Even when alignment with ground-truth information is explicitly evaluated, standard multi-label prediction metrics, typically binary accuracy, are often used despite their limitations in sparse settings (Panousis et al., 2024) and without considering their suitability as a proxy to interpretability. In many settings, ground-truth attributes are highly sparse; consequently, methods that predict a large number of inactive concepts can achieve deceptively high binary accuracy. Instead, it is crucial to assess which concepts are correctly inferred as active relative to the total number

of active concepts (i.e., the precision of the concepts used towards the downstream task) while simultaneously accounting for the imposed sparsity ratio and the performance of the model toward the downstream task.

Thus, in this work, we argue for a return to the initial drive behind concept-based approaches by explicitly analyzing the effect of modeling choices on interpretability and performance. To this end, we propose a new metric to measure the *clarity* of a concept-based representation. This metric captures the interplay between three desiderata in CBMs: *high sparsity*, to enable per-example inspection of the used concepts; *high concept prediction precision*, to ensure that the selected concepts are semantically correct while allowing for the selection of informative but non-comprehensive concept-based descriptions; and *strong downstream classification accuracy*, so that interpretability does not come at the expense of the downstream task performance. We consider two distinct CBM formulations: one based on explicit attribute prediction and the other grounded in Vision-Language Models, and systematically evaluate the impact of sparsity across three different sparsity-aware methods. Our contributions can be summarized as follows:

- We propose a systematic pipeline to objectively evaluate the interpretability-performance trade-off of concept-based representations that simultaneously considers: sparsity and correctness of the detected concepts, and task performance.
- We introduce a novel amortization scheme to enforce sparsity on a per-example basis for both ℓ_0 and ℓ_1 based approaches by selecting only relevant concepts.
- Through extensive experiments, we demonstrate that, contrary to claims that VLMs and sparsity inherently enhance interpretability, a trade-off exists between representational flexibility and interpretability in the learned concepts.

2. Related Work

Concept Bottleneck Models. Given a classification problem characterized by a dataset $\mathcal{D} = \{\mathbf{X}_n, \hat{\mathbf{y}}_n\}_{n=1}^N$ comprising N image/label pairs, where $\mathbf{X}_n \in \mathbb{R}^{I_H \times I_W \times c}$ and $\hat{\mathbf{y}}_n \in \{0, 1\}^C$, CBMs (Mahajan et al., 2011; Koh et al., 2020) aim at improving the interpretability of compute vision models solving this problem by first predicting a vector $\mathbf{a}_n = f_\theta(\mathbf{X}_n) \in [0, 1]^M$ of concept scores; these correspond to a *concept set* $A = \{a_1, \dots, a_M\}$, where every element is associated with a human-understandable concept. The score is related to the likelihood of the presence of such concept in the image, followed by a linear layer that maps the concept scores to the downstream task, $\mathbf{y}_n = \mathbf{W}_c^\top \mathbf{a}_n$. Training the concept predictor requires a dataset of image-concept labels, which has motivated the emergence of label-free approaches (Oikarinen et al., 2023; Yang et al., 2023)

that leverage pretrained VLMs, e.g., CLIP (Radford et al., 2021), to estimate the presence of concepts in an image.

Leakage in Concept Bottleneck Models. Information leakage, a phenomenon in which the model high jacks the concept bottleneck in order to directly encode information for the downstream task, is known to pose a big problem to the interpretability of CBMs (Margelou et al., 2021; Schoen et al., 2025), and can stem either from wrong concept predictions in the bottleneck or from nonsensical relations between the concepts and the downstream task. Leakage has been shown to be difficult to measure (Zarlenga et al., 2023), with some authors proposing to use occlusion of ground truth object parts to detect and correct it (Huang et al., 2024). Some methods to prevent leakage involve adding a non-interpretable side channel to the model (Havasi et al., 2022), releasing pressure from the concept predictor but turning the model into a partial black-box, or carefully choosing the concept set (Ruiz Luyten & van der Schaar, 2024), which is not always an option in real-world applications.

Sparsity in Concept Bottleneck Models. On top of raising concerns about the difficulty of learning a concept predictor, the authors of (Ramaswamy et al., 2023) point at another overlooked problem: large concept sets can render CBMs actually unintelligible to humans, with users preferring a handful of concepts per explanation. This has driven the development of sparsity-aware CBMs, where only a few concepts are selected to contribute to the downstream task, while the rest are effectively zeroed out. These methods focus on sparsifying either the concept bottleneck scores (Panousis et al., 2023; 2024) or the concept-class matrix that links concept scores to the downstream task (Yang et al., 2023; Schrodi et al., 2025), while some aim at inducing both types of sparsity simultaneously (Marcos et al., 2020).

3. Background on sparse representations

Sparsity-aware learning has a long history, spanning from early signal processing and compressed sensing to modern deep architectures. While a variety of methods exist, they all share a common principle: an underlying *sparse code* is assumed to exist that can adequately represent the data; this assumption is explicitly enforced during learning to enhance interpretability, efficiency, and generalization. In the context of machine learning, one of the most common approaches towards sparsity is the ℓ_1 regularization (Theodoridis, 2015), where the optimization process is given by:

$$\min_{\boldsymbol{\theta}} \frac{1}{N} \sum_{i=1}^N \mathcal{L}^{\text{task}}(f(\mathbf{x}_i; \boldsymbol{\theta}), y_i) + \lambda \|\boldsymbol{\theta}\|_1 \quad (1)$$

where $\|\boldsymbol{\theta}\|_1 = \sum_{j=1}^M |\theta_j|$ is the ℓ_1 norm of $\boldsymbol{\theta}$ and $\lambda \geq 0$ is a tunable parameter controlling the penalty contribution. A key property of the ℓ_1 constraint is that it promotes sparse

solutions, typically computed via coordinate descent. The ℓ_1 norm is simple, effective and easy to implement, which has contributed to its widespread adoption in modern ML. Nevertheless, more expressive priors exist that can further enhance interpretability. For instance, the ℓ_0 “norm” can enforce sparsity by directly counting non-zero parameters, potentially leading to even more precise sparse representations. However, the combinatorial nature of the ℓ_0 definition renders the optimization problem intractable. To bypass this issue, (Louizos et al., 2018) relax the discrete nature of the optimization, introducing a construction based on the *Hard Concrete* distribution.

The empirical loss minimization with ℓ_0 penalty reads:

$$\min_{\boldsymbol{\theta}} \frac{1}{N} \sum_{i=1}^N (\mathcal{L}^{\text{task}}(f(\mathbf{x}_i; \boldsymbol{\theta}, y_i)) + \lambda \|\boldsymbol{\theta}\|_0) \quad (2)$$

where $\|\boldsymbol{\theta}\|_0 = \sum_{j=1}^M \mathbb{I}[\theta_j \neq 0]$

We can reparameterize the parameter vector $\boldsymbol{\theta}$, s.t.:

$$\theta_j = \tilde{\theta}_j z_j, \quad (3)$$

where $z_j \in \{0, 1\}$, $\tilde{\theta}_j \neq 0$, $\|\boldsymbol{\theta}\|_0 = \sum_{j=1}^M z_j$

where $z_j, j = 1, \dots, M$ constitute auxiliary binary latent variables, that denote if each parameter is present or absent; thus, the ℓ_0 term now acts as a counter of the components that are active each time. By imposing an appropriate Bernoulli distribution on the latent variables \mathbf{z} , such that $z_j \sim \text{Bernoulli}(\pi_j), \forall j$, the empirical loss function can be written as follows (Louizos et al., 2018):

$$\mathbb{E}_{q(\mathbf{z}|\boldsymbol{\pi})} \left[\frac{1}{N} \left(\sum_{i=1}^N \mathcal{L}^{\text{task}}(f(\mathbf{x}_i; \mathbf{z} \cdot \tilde{\boldsymbol{\theta}}, y_i)) \right) \right] + \lambda \sum_{j=1}^M \pi_j \quad (4)$$

Again, the discrete nature of \mathbf{z} renders gradient-based optimization inefficient, with REINFORCE estimators (Williams, 1992) suffering from high variance, while the Concrete distribution (Maddison et al., 2017; Jang et al., 2017) and the Straight Through estimators suffer from their own drawbacks, i.e., biased gradients and not exact zeroes respectively. Thus, the authors introduce a continuous random variable \mathbf{s} , governed by a distribution $q(\mathbf{s})$ and parameters $\boldsymbol{\phi}$, followed by a hard-sigmoid rectification. This hierarchical construction reads:

$$\mathbf{s} \sim q(\mathbf{s}|\boldsymbol{\phi}) \quad (5)$$

$$\mathbf{z} = \min(\mathbf{1}, \max(\mathbf{0}, \mathbf{s})), \quad (6)$$

yielding the so-called *Hard Concrete* distribution. In practice, the Hard Concrete distribution treats \mathbf{s} as a continuous

relaxation of the Bernoulli distribution, parameterized by $\boldsymbol{\phi} = (\log \alpha, \beta)$, where $\log \alpha$ is the location and β is the temperature, yielding the following sampling procedure:

$$s = \sigma((\log u - \log(1 - u) + \log \alpha)/\beta) \quad (7)$$

$$\bar{s} = s(\zeta - \gamma) + \gamma \quad (8)$$

$$z = \min(1, \max(0, \bar{s})) \quad (9)$$

where $u \sim \mathcal{U}(0, 1)$, $\sigma(\cdot) = \text{Sigmoid}(\cdot)$, and $\gamma < 0$ and $\zeta > 1$ can be used to stretch the arising distribution to the (γ, ζ) interval. The final objective function comprises the *error* and the *complexity loss* (Louizos et al., 2018); it is estimated through MC sampling with L samples, reads:

$$\mathcal{L} = \frac{1}{L} \sum_{l=1}^L \left(\frac{1}{N} \sum_{i=1}^N \mathcal{L}^{\text{task}}(f(\mathbf{x}_i; \tilde{\boldsymbol{\theta}} \cdot \mathbf{z}^{(l)}), y_i) \right) + \sum_{j=1}^M \text{Sigmoid} \left(\log \alpha_j - \beta \log \frac{-\gamma}{\zeta} \right) \quad (10)$$

Direct optimization of the ℓ_0 norm is combinatorially hard, and methods like Hard Concrete provide continuous relaxations to make it differentiable for gradient-based optimization. An alternative approach is to model sparsity probabilistically using Bernoulli variables, where each parameter is stochastically “switched on/off,” enabling principled learning of sparse structures in a fully differentiable framework.

Drawing inspiration from latent feature models (Griffiths & Ghahramani, 2011), we can introduce a set of auxiliary binary latent variables $\mathbf{z} \in \{0, 1\}^M$, that dictate which components are active at any given time. In analogy to the ℓ_0 formulation, we can reparameterize the parameter vector $\boldsymbol{\theta}$, such that:

$$\theta_j = \tilde{\theta}_j \cdot z_j, \quad z_j \in \{0, 1\} \quad (11)$$

We can now impose an appropriate prior on these latent variables, i.e., a Bernoulli distribution, such that $\mathbf{z} \sim \text{Bernoulli}(\tilde{\boldsymbol{\pi}})$ and perform inference on both the parameter vector $\boldsymbol{\theta}$ and the latent variables \mathbf{z} . Using a mean-field approach variational posterior $q(\mathbf{z}|\boldsymbol{\pi}) = \text{Bernoulli}(\boldsymbol{\pi})$ (Beal, 2003; Wainwright & Jordan, 2008), the Evidence Lower Bound (ELBO) expression reads:

$$\text{ELBO} = \mathbb{E}_{q(\mathbf{z}|\boldsymbol{\pi})} \left[\frac{1}{N} \sum_{i=1}^N \mathcal{L}(f(\mathbf{x}_i; \tilde{\boldsymbol{\theta}} \cdot \mathbf{z}), y_i) \right] - KL[q(\mathbf{z}|\boldsymbol{\pi})||p(\mathbf{z}|\tilde{\boldsymbol{\pi}})]. \quad (12)$$

By placing a suitable sparsity-inducing prior on \mathbf{z} , i.e., $\mathbf{z} \sim \text{Bernoulli}(\tilde{\boldsymbol{\pi}})$, we encourage only a subset of parameters to be active while performing joint inference over $\boldsymbol{\theta}$ and \mathbf{z} . The ELBO is typically optimized via MC sampling.

Building on these definitions of the three sparsity-aware formulations, we now turn to their use in designing per-example sparsity-aware concept selection mechanisms.

4. Proposed Framework

In this work, we focus on Concept Bottleneck Models and specifically concept-based classification. Let us denote by $\mathcal{D} = \{\mathbf{X}_i, y_i\}_{i=1}^N$, a dataset comprising N examples, each belonging to a class $c \in C$, such that $y_i \in \{0, 1\}^C$. We additionally consider a *concept set* $A = \{a_1, \dots, a_M\}$, which typically comprises human-interpretable notions, usually expressed by text or attribute presence. Within this frame of reference, we first aim to train a predictor that outputs the concept scores for each image, which is then used to classify each example; thus, we create an interpretable bottleneck to drive the downstream task. Assuming a transformation $f_{\text{pred}}(\mathbf{X}_i) \in (0, 1)^M$ that predicts, for each image, the concept scores, and a classification weight matrix $\mathbf{W}_c \in \mathbb{R}^{M \times C}$, the optimization process reads:

$$\min_{\mathbf{W}_c} \mathcal{L}_c = \sum_{i=1}^N \text{CE}(\mathbf{W}_c^\top f_{\text{pred}}(\mathbf{X}_i), y_i) \quad (13)$$

The predictor is commonly a neural network that is pre-trained by minimizing the binary cross-entropy between its sigmoided predictions and the ground-truth concept labels; during concept-based classification, it remains frozen.

However, this formulation of CBMs is considered very restrictive. Indeed, annotating concepts for a particular dataset and concept set is a very strenuous process, while the presence or not of concepts is often open to human interpretation. To this end, several works aim to bypass the need for ground-truth information by employing VLMs (Yang et al., 2023; Oikarinen et al., 2023; Panousis et al., 2023). In this setting, we do not need to train a predictor; instead, by exploiting the zero-shot capabilities of VLMs we can obtain the similarity between any image in the dataset and any potential concept set. Denoting by $E_I(\mathbf{X}_i) \in \mathbb{R}^K$, $E_T(\mathbf{A}) \in \mathbb{R}^{M \times K}$, the K -dimensional embeddings of the image and of the concept set, respectively, obtained through the encoders of a considered VLM, the concept scores can be predicted as:

$$f_{\text{VLM}}(\mathbf{X}_i) = E_I(\mathbf{X}_i) E_T(\mathbf{A})^\top \in \mathbb{R}^M \quad (14)$$

with the classification loss being similar to Eq. (13), where instead of f_{pred} , we use f_{VLM} .

Although VLMs have considerably increased the flexibility of CBMs, at the same time, they have harmed the interpretability efforts by allowing the usage of massive concept sets while basing the inference process on the implicit concept similarity provided by them. To this end, and following relevant VLM-based CBM literature (Yang et al., 2023;

Oikarinen et al., 2023; Panousis et al., 2023; 2024), we consider a sparsification approach, aiming to drastically reduce the *per-example* number of active concepts to facilitate interpretability of the individual emerging representations.

To this effect, we consider auxiliary binary latent variables $\mathbf{z}_i \in \{0, 1\}^M, \forall i$; these denote the presence or absence of the concepts $\{a_m\}_{m=1}^M \in \mathbf{A}$ for each example, by masking the corresponding entries during classification, i.e.,

$$\hat{\mathbf{y}}_i = (\mathbf{z}_i \cdot \mathbf{W}_c)^\top f_{\text{pred/VLM}}(\mathbf{X}_i) \quad (15)$$

We can rely on different estimation approaches to infer the auxiliary latent variables \mathbf{Z} . Ideally, these latent variables should be highly sparse, yielding a representation that is both compact and potentially interpretable; thus, we want to induce sparsity that not only facilitates the downstream task but also enables a per-example concept investigation and analysis of the emergent behavior of concept selection. To this end, we build on the three sparsification methods discussed on the previous section: ℓ_0 , ℓ_1 , and Bernoulli-based formulations. For this purpose, we introduce an amortized version for both the ℓ_1 and ℓ_0 formulation (Louizos et al., 2018), similar to the Bernoulli-based scheme proposed in (Panousis et al., 2023), enabling efficient inference of the sparse latent variables per example. Specifically, we consider a single amortization matrix $\mathbf{W}_s \in \mathbb{R}^{K \times M}$ to compute the latent variables \mathbf{Z} , which in turn act as *concept selectors* towards classification. To drive the computation of the latent variables, we exploit the image encoder of the considered VLM, yielding the following intermediate representation $\hat{\Phi}$:

$$\hat{\Phi} = \mathbf{W}_s^\top E_I(\mathbf{X}) \in \mathbb{R}^{N \times M} \quad (16)$$

This representation can be seen as the *unnormalized concept scores* that we can now transform according to the sparsity-aware method considered.

For the ℓ_1 -based method, we transform these logits via a sigmoid transformation $\sigma(\cdot) = \text{Sigmoid}(\cdot)$, s.t.:

$$\mathbf{Z}_{\ell_1} = \sigma(\hat{\Phi}) \quad (17)$$

For the ℓ_0 , we can rewrite the sampling procedure as:

$$\begin{aligned} u &= \mathcal{U}(0, 1), \quad s = \sigma((\log u - \log(1 - u) + \hat{\Phi})/\beta) \\ \bar{\sigma} &= s(\zeta - \gamma) + \gamma \\ \mathbf{Z}_{\ell_0} &= \min(1, \max(0, \bar{s})) \end{aligned} \quad (18)$$

And finally, for the Bernoulli-based procedure:

$$\mathbf{Z}_{\text{Bernoulli}} = \text{Bernoulli}(\mathbf{Z} | \sigma(\hat{\Phi})) \quad (19)$$

The definition of the auxiliary latent variables \mathbf{Z} for all three sparsity-aware methods is now concluded; we now turn to the training procedure and describe how the latent variables and model parameters are jointly learned.

Training. We consider two alternative backbones for computing concept scores. One is based on a VLM, where concept scores are directly obtained using Eq. (14), and the other relies on an *attribute predictor* as described in Eq. (13). Specifically, we train a predictor model that takes as input an image’s embedding stemming from the image encoder of a VLM and outputs the concept scores; it comprises a single linear layer $\mathbf{W}_{\text{pred}} \in \mathbb{R}^{K \times M}$ followed by a sigmoid non-linearity, while optimizing the binary cross entropy between the predictions and the ground-truth attributes.

Given a trained predictor or a VLM that outputs the concept scores for each example, all considered sparsity-aware concept-based classification models comprise two learnable parameters: (i) the amortization matrix $\mathbf{W}_s \in \mathbb{R}^{K \times M}$ and (ii) the classification matrix $\mathbf{W}_c \in \mathbb{R}^{M \times C}$. For each method, the final loss involves two terms, the classification loss and the regularization/penalty term stemming from the corresponding sparsification process. For the ℓ_1 -based method, we impose the regularization penalty on the activations \mathbf{z}_i themselves, since the goal is to penalize the concept activations rather than the amortization matrix itself. For ℓ_0 -based sparsity, the penalty corresponds to the second term in Eq. (10), where $\log \alpha = \mathbf{W}_s^\top E_I(\mathbf{X}) \in \mathbb{R}^{N \times M}$, s.t.:

$$\mathcal{L}_{\ell_0}^{\text{penalty}} = \frac{1}{N} \sum_{i,m}^{N,M} \sigma \left(\mathbf{W}_s^\top E_I(\mathbf{X}) - \beta \log \frac{-\gamma}{\zeta} \right) \quad (20)$$

Finally, for the Bernoulli-based formulation, and since Bernoulli is not amenable to the reparameterization trick, we consider its relaxation based on the Concrete distribution (Maddison et al., 2017; Jang et al., 2017) to draw samples from the approximate posterior during training; for the “penalty”, we compute the KL divergence between a fixed sparsity-inducing prior and the Bernoulli posterior, thus optimizing the loss provided in Eq. (12).

To infer the latent variables \mathbf{Z} for each method, we only use the classification signal stemming from their corresponding loss optimizing both \mathbf{W}_s and \mathbf{W}_c in an end-to-end fashion; then, we freeze the amortization matrix \mathbf{W}_s and re-train the classification matrix \mathbf{W}_c with different *thresholds* to properly assess the potency of the sparse codes and obtain the final classification performance as detailed next.

Inference. Having trained \mathbf{W}_s , we can compute, for each method, the active concepts per example. Specifically, we introduce a threshold τ that can be used to determine if a concept is active or not for an example i , via its inferred auxiliary variable \mathbf{z}_i . For ℓ_1 , we can directly threshold the indicators \mathbf{Z}_{ℓ_1} computed via Eq. (17), s.t.:

$$\tilde{z}_{\ell_1}^m = \begin{cases} 1, & \text{if } [\sigma(\mathbf{W}_s^\top E_I(\mathbf{X}_{\text{test}}))]_m > \tau \\ 0, & \text{otherwise} \end{cases} \quad (21)$$

For ℓ_0 , the logit transformation during inference reads:

$$\tilde{z}_{\ell_0} = \min(1, \max(0, \sigma(E_I(\mathbf{X}_{\text{test}}) \mathbf{W}_s^\top))(\zeta - \gamma) + \gamma) \quad (22)$$

Thus, we can use τ as before. For the Bernoulli-based formulation, we can directly threshold the inferred amortized probabilities of the Bernoulli distribution, leading to a similar thresholding rule based on the inner product between the amortization matrix and the test input.

Evaluation. We argue that, for a concept-based model to be truly interpretable, three criteria must be simultaneously satisfied: *high sparsity*, to enable per-example inspection of the active concepts; *high precision*, to ensure that the selected concepts are semantically correct; and *strong classification accuracy*, so that interpretability does not come at the expense of performance in the context of the downstream task. To capture the interplay and trade-offs among these competing objectives, we introduce the notion of *clarity*, a novel metric designed to quantify interpretability in concept-based models that reads:

$$\begin{aligned} \text{Clarity} &= H(\text{Acc}, \text{Sparsity}, \text{Precision}) \\ &= \frac{3 \cdot \text{Acc} \cdot \text{Sparsity} \cdot \text{Prec}}{\text{Acc} \cdot \text{Sparsity} + \text{Acc} \cdot \text{Prec} + \text{Sparsity} \cdot \text{Prec}} \end{aligned} \quad (23)$$

We adopt the harmonic mean to define clarity as it explicitly penalizes imbalances among sparsity, precision, and classification accuracy, ensuring that a high clarity score is achieved only when all three components are simultaneously strong; in contrast, even when a single component is small, it yields a low score, capturing the trade-off between these interdependent quantities.

5. Experimental Evaluation and Discussion

Experimental Setup. We consider two benchmark datasets with ground-truth attributes, namely CUB (Wah et al., 2011) and SUN (Xiao et al., 2010). These datasets span diverse characteristics, including number of examples, classes and attributes; CUB comprises 11780 examples divided into 200 classes with per-example ground-truth attributes from a pool of 312, while SUN comprises 14340 examples, spanned across 700 classes with a pool of 102 attributes. CUB attributes are highly visual attributes, e.g., *wing color black, undeparts color orange*; the same holds for SUN, although it also includes a few non-visual cues, e.g., *scary, research, stressful*. For each dataset, ground truth information is provided via per-example attribute presence information. When using a VLM to compute the relation between the images and the attributes, we consider as concept set the ground truth attributes provided in each dataset; thus, in this case we consider no explicit ground-truth information and rely on the zero-shot capabilities of VLMs as commonly done in the related literature. We split the CUB

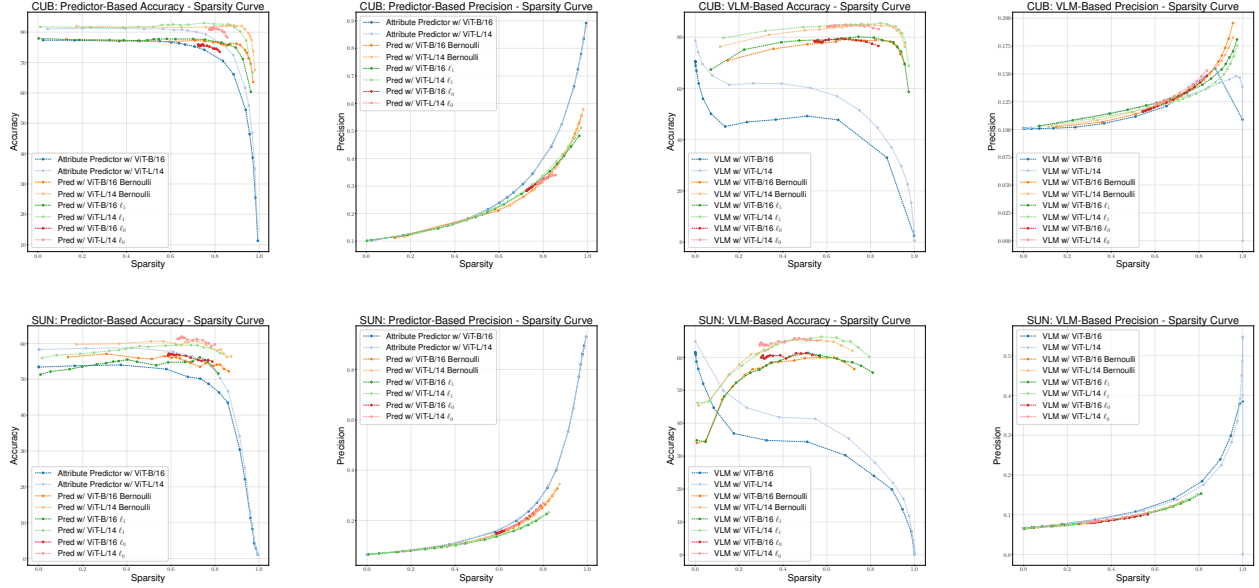


Figure 1. Accuracy-Sparsity and Precision-Sparsity Curves for the CUB (top) and SUN (bottom) datasets. From left to right, we report results for predictor-based methods (first two plots) and VLM-based methods (last two plots). For both methods, all sparsity-inducing approaches maintain strong classification performance even at high sparsity levels. For the VLM-based setting, we observe a significant increase in classification accuracy when employing sparsity-aware methods. This suggests that, despite the limited zero-shot attribute prediction capabilities of CLIP in this scenario, appropriate concept selection can recover substantial discriminative power for the downstream task. At the same time, increased sparsity consistently leads to higher precision in the resulting representations.

dataset according to the typical split, i.e., 5990 examples for training, 5790 for testing, while for SUN we choose a 80% – 20% split, the same for all methods.

Training Details. To train the *attribute predictor* and drive the computation of the auxiliary binary indicators Z for each of the considered methods, we exploit image embeddings stemming from the image encoder of a VLM, and specifically CLIP. We consider two commonly used CLIP variants, i.e., ViT-B/16 and ViT-L/14; this decision also facilitates the investigation of how different embeddings affect the inferred representations. To avoid re-computing the embeddings at every iteration, we pre-compute them and store them in an efficient format for repeated use. For the *predictor-based* models, we train the attribute predictor for a fixed number of epochs for all combinations of datasets and embedding backbones. For the *VLM-based* models, we compute similarities with text embeddings corresponding to the considered concept set. In all cases, the training of the binary indicators Z is performed by minimizing the corresponding sparsity-aware loss for each method over 1500 epochs across all experimental settings. After learning the amortization matrix for each method, we re-train the classification layer, i.e., W_c , using different thresholds and for 200 epochs each, to evaluate how effectively the sparse codes support classification, while ensuring a fair basis for computing the interpretability metrics.

Table 1. Attribute prediction performance with respect to ground-truth attribute information. We use only example-wise attribute information for training the attribute predictor, while for CLIP we consider the similarity between the image and text embeddings.

Model	Dataset	Backbone	mAP	AUC
Predictor	CUB	ViT-B/16	61.05	0.882
	CUB	ViT-L/14	61.19	0.859
	SUN	ViT-B/16	73.60	0.953
	SUN	ViT-L/14	74.30	0.954
VLM	CUB	ViT-B/16	16.32	0.540
	CUB	ViT-L/14	14.91	0.565
	SUN	ViT-B/16	31.82	0.748
	SUN	ViT-L/14	29.96	0.734

Baseline Results. We begin our experimental result analysis with the assessment of the concept prediction backbones. In Table 1, the attribute prediction performance for the two types of concept score prediction models, Predictor-based and VLM-based, across the two benchmark datasets and using the two backbone architectures for obtaining the embeddings, are reported. For the evaluation metrics in this context, we consider the mean Average Precision (mAP), which captures the overall ranking quality of the predicted attributes, and the Area Under the ROC Curve (AUC).

Therein, we observe that predictor-based models consistently outperform their VLM-based counterparts across both datasets and backbone architectures. This is expected, as models trained with explicit attribute supervision produce

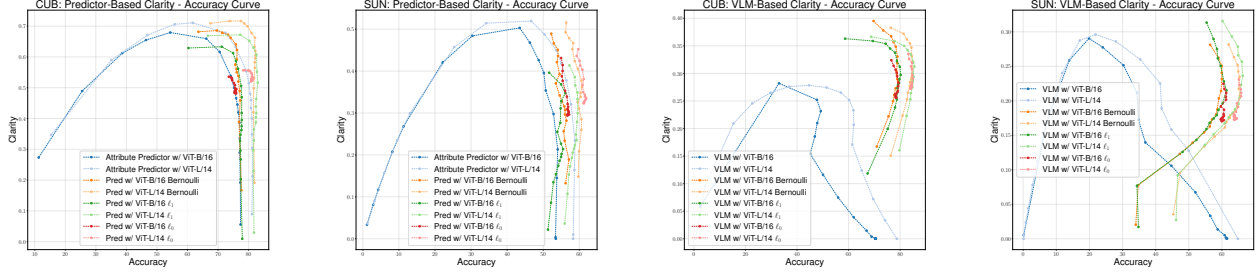


Figure 2. Clarity-Accuracy Curves for both datasets. From left to right, we report the results for predictor-based methods (first two plots) and VLM-based methods (last two plots). While all methods can achieve similar classification accuracy, they do so at widely different clarity levels, highlighting that strong task performance does not guarantee interpretable representations.

more accurate attribute predictions compared to the zero-shot capabilities of VLMs in these settings. Both methods perform better on the SUN dataset than on CUB, reflecting on the nature of the two datasets: SUN comprises 102 scene-level attributes, while the 312 CUB attributes are more fine-grained and harder to discriminate. Notably for CUB, the VLM-based approach achieves near-random performance, highlighting a potential limitation of its zero-shot properties in specialized, fine-grained domains. Finally, the results suggest that backbone size has limited impact on the final performance for both methods, indicating that increasing model capacity does not yield substantial improvements.

Concept Selection with Sparsity-aware Methods. We begin our analysis by examining classification performance as a function of sparsity for both predictor- and VLM-based approaches, depicted in Fig. 1. We observe that, in terms of classification accuracy, predictor- and VLM-based methods achieve comparable performance, despite the previously observed deficiencies of VLM-based models in attribute prediction. This indicates that accurate concept predictions are not strictly required for strong downstream performance, provided that the resulting representations capture discriminative information. In this setting, using a more expressive embedding backbone leads to a noticeable improvement in task performance, likely due to its increased representational capacity and ability to encode richer semantic information. Moreover, all sparsity-inducing methods achieve comparable classification performance at comparable sparsity levels, suggesting that the choice of sparsification approach has limited impact on task accuracy once sparsity is controlled. Importantly, all sparsity-aware methods substantially outperform a naive thresholding of the raw concept scores—for example, VLM w/ ViT-B/16. In the same figure, we plot the precision as a function of sparsity. A consistent pattern emerges across all methods: increasing sparsity generally leads to higher precision, indicating that the concept selection mechanisms assign higher scores to correctly predicted concepts. The Bernoulli-based formulation exhibits a slight advantage, while the choice of backbone has only a modest

effect on precision, suggesting that backbone capacity is not a major determinant in this setting.

However, from these plots, it is not straightforward to determine which model is “best” in terms of interpretability. This is where the notion of clarity becomes crucial. In Fig. 2, we plot clarity as a function of task performance, revealing a striking pattern: while all methods can achieve similar classification accuracy, they do so at widely different levels of clarity. This indicates that achieving strong downstream performance does not guarantee interpretable representations, and highlights the importance of explicitly evaluating interpretability metrics such as sparsity and precision alongside task accuracy when comparing sparsity-aware methods. Ideally, a method should lie in the upper-right region of such a graph, corresponding to high sparsity, high precision, and strong classification performance. In this instance, the Bernoulli-based method performs favorably across most settings, with the exception of the VLM-based formulation on the SUN dataset, where it is outperformed by the ℓ_1 regularization. Importantly, we do not advocate for a single best-performing method. Different sparsity-inducing approaches may be more optimally constructed or tuned to achieve higher clarity under specific modeling choices. While we explored a range of configurations for all methods, the reported results are not exhaustive and should be viewed as indicative rather than definitive.

To better quantify differences in model interpretability, Table 2 reports the results for all methods based on the maximum achieved clarity. We report classification accuracy, sparsity (measured as the average number of active concepts per example), and precision. These results highlight the importance of evaluating interpretability with metrics beyond just sparsity and task performance. In many cases, the model selected for maximum clarity is not the one with the highest classification accuracy. For instance, the predictor-based Bernoulli configuration achieves the highest clarity on CUB; although it does not attain the best accuracy or sparsity overall, it achieves the highest precision while balancing

Table 2. Results of sparsity-inducing methods on CUB and SUN datasets. Metrics for CUB and SUN are reported side by side. For each combination of embedding architecture, backbone and method, we report the models with the highest clarity, along with their classification accuracy, average active concepts per sample, the attribute prediction precision and binary accuracy.

Embed.	Backbone	Method	CUB					SUN				
			Clarity	Class Acc	Avg Act	Attr Precision	Attr BinAcc	Clarity	Class Acc	Avg Act	Attr Precision	Attr BinAcc
ViT-B/16	VLM	ℓ_1	0.363	58.65	0.02	0.1808	88.20	0.313	55.37	0.190	0.1531	80.20
		ℓ_0	0.324	76.61	0.162	0.148	78.30	0.225	60.46	0.434	0.1007	58.85
		Bernoulli	0.395	69.69	0.045	0.1956	87.16	0.281	56.45	0.274	0.133	73.32
	Predictor	ℓ_1	0.633	71.20	0.073	0.444	89.06	0.396	51.64	0.184	0.2267	83.33
		ℓ_0	0.536	73.50	0.179	0.3309	83.86	0.431	54.95	0.212	0.2585	83.18
		Bernoulli	0.686	69.64	0.038	0.5269	90.10	0.489	52.23	0.137	0.3270	88.69
ViT-L/14	VLM	ℓ_1	0.367	68.75	0.026	0.1753	88.22	0.316	60.18	0.207	0.1519	79.04
		ℓ_0	0.335	83.21	0.163	0.1528	78.49	0.231	65.13	0.443	0.1035	58.33
		Bernoulli	0.383	76.35	0.044	0.1825	87.12	0.282	62.03	0.282	0.1308	72.63
	Predictor	ℓ_1	0.672	77.28	0.059	0.4741	89.59	0.414	57.25	0.175	0.2329	84.08
		ℓ_0	0.557	79.95	0.157	0.3389	84.85	0.452	59.73	0.199	0.2695	84.24
		Bernoulli	0.717	77.48	0.034	0.5377	90.15	0.515	56.40	0.126	0.3450	89.50

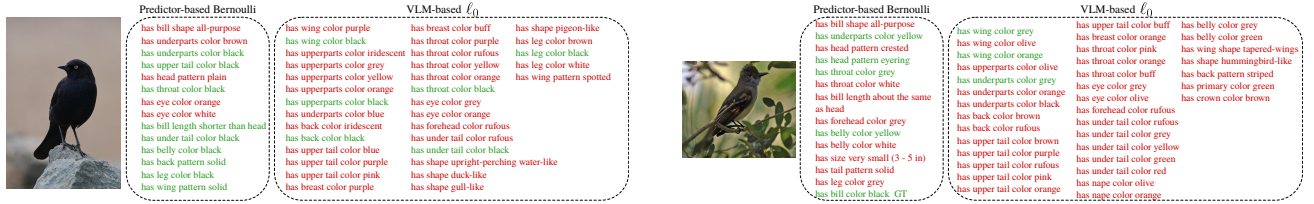


Figure 3. Visualization of selected concepts for two examples from the CUB dataset by selecting the method with the best clarity (predictor-based Bernoulli) versus the one with the best performance (VLM-based ℓ_0). Green highlighting denotes concepts that are present in the ground truth. **Left:** Brewer Blackbird example with 28 ground-truth active concepts. **Right:** Great Crested Flycatcher example with 30 ground-truth active concepts. Similar trends are observed in both cases, with the Bernoulli method selecting fewer, more precise concepts, and the ℓ_0 method selecting a larger set with lower precision.

all relevant metrics. Conversely, for the VLM-based ℓ_1 , the model selected for maximum clarity may be sub-optimal in terms of classification accuracy, yet it exhibits superior sparsity and precision, yielding higher overall clarity than the ℓ_0 counterpart, which, despite strong task performance, activates more concepts per example and achieves lower concept precision. In the same table, we also report the computed binary accuracy, a metric often used to evaluate interpretability in concept-based models. We observe that binary accuracy can be misleading: in many cases, models achieve similar binary accuracy despite exhibiting substantial differences in key interpretability components, such as precision and sparsity. This is particularly evident for the VLM-based methods, where high binary accuracy does not necessarily correspond to a model with meaningful or sparse concept activations.

Finally, in Fig. 3, we visualize the selected concepts for two representative models on two examples from the CUB dataset: the model achieving the highest clarity (Predictor-based Bernoulli) and the model achieving the highest classification accuracy (VLM-based ℓ_0), as reported in Table 2. We observe that the high-clarity model selects a compact set of concepts with high precision, whereas the high-accuracy model activates a large number of concepts that do not align with the ground-truth annotations, further showcasing the need for a more in-depth evaluation of concept-based mod-

els with respect to interpretability. Further qualitative results are provided in the appendix.

6. Limitations & Conclusions

A limitation of the proposed pipeline is its reliance on ground-truth concept annotations to evaluate clarity. However, we argue that such analyses constitute an important first step toward the development of more interpretable architectures. Several datasets with ground-truth annotations already exist, enabling principled empirical evaluations in which sparsity can be assessed in a meaningful way, rather than imposed for sparsity’s sake. These controlled settings can then serve as a foundation for extending the analysis to more complex datasets and application domains. A promising direction for future work is the use of more informative priors, particularly in the Bernoulli-based formulation, where approximate individual or aggregate concept presence scores, often easier to obtain than per-example annotations, can guide sparsification and improve interpretability.

In this work, we introduced a principled framework for the systematic evaluation of sparsity-aware concept-based methods. We proposed two novel amortized formulations for per-example attribute selection based on the ℓ_0 and ℓ_1 constraints, and introduced *clarity*, a metric that jointly captures sparsity, precision, and downstream task performance.

Through extensive experiments on benchmark datasets with attribute-prediction backbones, we showed that sparsity-aware methods can exhibit markedly different behaviors even at comparable accuracy levels, revealing an inherent trade-off between model flexibility, sparsity, and precision.

Impact Statement

This work aims to address the challenge of evaluating the interpretability of sparsity-aware concept bottleneck models. To this end, we consider benchmark datasets, model architectures, and sparsity-inducing methods in order to quantify the impact of various design choices on the resulting clarity of the learned representations. By doing so, this work seeks to advance the field of explainable artificial intelligence by making the decision-making processes of modern architectures more transparent. We do not foresee any apparent negative societal consequences arising from this work that warrant specific discussion.

References

- Beal, M. J. *Variational Algorithms for Approximate Bayesian Inference*. PhD thesis, Gatsby Computational Neuroscience Unit, University College London, 2003.
- Griffiths, T. L. and Ghahramani, Z. The indian buffet process: An introduction and review. *Journal of Machine Learning Research*, 2011.
- Havasi, M., Parbhoo, S., and Doshi-Velez, F. Addressing leakage in concept bottleneck models. *Advances in Neural Information Processing Systems*, 35:23386–23397, 2022.
- Huang, Q., Song, J., Hu, J., Zhang, H., Wang, Y., and Song, M. On the concept trustworthiness in concept bottleneck models. In *Proceedings of the AAAI Conference on Artificial Intelligence*, volume 38, pp. 21161–21168, 2024.
- Jang, E., Gu, S., and Poole, B. Categorical reparametrization with gumbel-softmax. In *Proc. ICLR*, 2017.
- Kingma, D. P. and Welling, M. Auto-encoding variational bayes. In *Proc. ICLR*, 2014.
- Koh, P. W., Nguyen, T., Tang, Y. S., Mussmann, S., Pierson, E., Kim, B., and Liang, P. Concept bottleneck models. In *Proc. ICML*, 2020.
- Louizos, C., Welling, M., and Kingma, D. P. Learning sparse neural networks through l_0 regularization. In *Proc. ICLR*, 2018.
- Maddison, C. J., Mnih, A., and Teh, Y. W. The concrete distribution: A continuous relaxation of discrete random variables. In *Proc. ICLR*, 2017.
- Mahajan, D., Sellamanickam, S., and Nair, V. A joint learning framework for attribute models and object descriptions. In *Proc. ICCV*, 2011.
- Marcos, D., Fong, R., Lobry, S., Flamary, R., Courty, N., and Tuia, D. Contextual semantic interpretability. In *Proceedings of the Asian Conference on Computer Vision*, 2020.
- Margelioiu, A., Ashman, M., Bhatt, U., Chen, Y., Jamnik, M., and Weller, A. Do concept bottleneck models learn as intended? *arXiv preprint arXiv:2105.04289*, 2021.
- Oikarinen, T., Das, S., Nguyen, L. M., and Weng, T.-W. Label-free concept bottleneck models. In *Proc. ICLR*, 2023.
- Panousis, K. P., Ienco, D., and Marcos, D. Sparse linear concept discovery models. In *Proc. ICCV Workshops*, 2023.
- Panousis, K. P., Ienco, D., and Marcos, D. Coarse-to-fine concept bottleneck models. In *Proc. NeurIPS*, 2024.
- Radford, A., Kim, J. W., Hallacy, C., Ramesh, A., Goh, G., Agarwal, S., Sastry, G., Askell, A., Mishkin, P., Clark, J., Krueger, G., and Sutskever, I. Learning transferable visual models from natural language supervision. In *ICML*, 2021.
- Ramaswamy, V. V., Kim, S. S., Fong, R., and Russakovsky, O. Overlooked factors in concept-based explanations: Dataset choice, concept learnability, and human capability. In *Proceedings of the IEEE/CVF Conference on Computer Vision and Pattern Recognition*, pp. 10932–10941, 2023.
- Ruiz Luyten, M. and van der Schaar, M. A theoretical design of concept sets: improving the predictability of concept bottleneck models. *Advances in Neural Information Processing Systems*, 37:100160–100195, 2024.
- Schoen, R., Abeloos, B., and Herbin, S. Measuring and addressing information leakage in concept bottleneck models. In *Proceedings of the IEEE/CVF International Conference on Computer Vision*, pp. 624–632, 2025.
- Schrodi, S., Schur, J., Argus, M., and Brox, T. Selective concept bottleneck models without predefined concepts. *Transactions on Machine Learning Research*, 2025.
- Theodoridis, S. *Machine Learning: A Bayesian and Optimization Perspective*. Academic Press, 2015. ISBN 978-0128015223.
- Wah, C., Branson, S., Welinder, P., Perona, P., and Belongie, S. The caltech-ucsd birds-200-2011 dataset. Technical report, 2011.

Wainwright, M. J. and Jordan, M. I. *Graphical Models, Exponential Families, and Variational Inference*. 2008.

Williams, R. J. Simple statistical gradient-following algorithms for connectionist reinforcement learning. *Machine Learning*, 8:229–256, 1992.

Xiao, J., Hays, J., Ehinger, K. A., Oliva, A., and Torralba, A. Sun database: Large-scale scene recognition from abbey to zoo. In *Proc. CVPR*, 2010.

Yang, Y., Panagopoulou, A., Zhou, S., Jin, D., Callison-Burch, C., and Yatskar, M. Language in a bottle: Language model guided concept bottlenecks for interpretable image classification. In *Proc. CVPR*, 2023.

Zarlenga, M. E., Barbiero, P., Shams, Z., Kazhdan, D., Bhatt, U., Weller, A., and Jamnik, M. Towards robust metrics for concept representation evaluation. In *Proceedings of the AAAI Conference on Artificial Intelligence*, volume 37, pp. 11791–11799, 2023.

A. Experimental Details.

For our experiments, we set the Bernoulli prior to a very small value, 10^{-4} , to strongly enforce sparsity. For methods that use the continuous relaxation of the Bernoulli distribution (i.e., Bernoulli- and ℓ_0 -based methods), we use a temperature of 0.1, while we set $\gamma = -0.1$ and $\zeta = 1.1$ for the HardConcrete distribution following (Louizos et al., 2018).

For both Bernoulli and Hard Concrete based experiments, we compute the loss using $L = 1$ sample. We did not observe any impact when using more samples.

We explored a wide range of relevant hyperparameters for all methods: learning rates $[10^{-2}, 5 \cdot 10^{-3}, 10^{-3}, 5 \cdot 10^{-4}, 10^{-4}]$, λ for ℓ_1 regularization $[10^{-5}, 5 \cdot 10^{-5}, 10^{-6}, 5 \cdot 10^{-6}, 10^{-7}]$, and λ for ℓ_0 -related sparsity $[10^{-2}, 5 \cdot 10^{-2}, 10^{-1}, 5 \cdot 10^{-1}, 1]$. Additionally, we evaluated a wide range of thresholds: $[10^{-4}, 10^{-3}, 5 \cdot 10^{-3}, 10^{-2}, 2 \cdot 10^{-2}, 3 \cdot 10^{-2}, 4 \cdot 10^{-2}, 5 \cdot 10^{-2}, 7 \cdot 10^{-2}, 10^{-1}, 2 \cdot 10^{-1}, 3 \cdot 10^{-1}, 5 \cdot 10^{-1}, 6 \cdot 10^{-1}, 7 \cdot 10^{-1}, 8 \cdot 10^{-1}, 9 \cdot 10^{-1}]$.

For the image/text encoders, we use ViT-B/16 and ViT-L/14, which produce embeddings of dimensionality 512 and 768, respectively.

All models were trained using the Adam optimizer without any complex annealing schedules, on a single NVIDIA A6000 GPU with 48GB of VRAM.

A.1. Concrete Relaxation

Since, Bernoulli samples cannot be expressed via the reparameterization trick (Kingma & Welling, 2014), we turn to its continuous relaxation, i.e., the Concrete distribution (Maddison et al., 2017; Jang et al., 2017).

Let π_i denote the probabilities of $q(z_i)$ for $i = 1, \dots, N$. We can obtain reparameterized samples $\hat{z}_i \in (0, 1)^M$ from the continuous relaxation as

$$\hat{z}_i = \frac{1}{1 + \exp(-(\log \pi_i + L) / \beta)}, \quad (24)$$

where $L \in \mathbb{R}$ is a sample from the Logistic distribution, defined as

$$L = \log U - \log(1 - U), \quad U \sim \text{Uniform}(0, 1), \quad (25)$$

and β is the *temperature* parameter controlling the smoothness of the relaxation: higher β values produce samples closer to uniform, while lower values yield samples closer to binary. In all experiments, we set $\beta = 0.1$. During inference, the discrete Bernoulli distribution can be used to directly draw binary indicators.

B. Additional Visualizations

Predictor-based Bernoulli	VL-based ℓ_1	Predictor-based Bernoulli	VL-based ℓ_1
 <ul style="list-style-type: none"> has underparts color grey has breast pattern spotted has head pattern eyebrow has belly color black has throat color black has belly color buff has back pattern spotted has tail pattern spotted has tail pattern striped has belly pattern spotted has leg color buff has wing pattern spotted 	<ul style="list-style-type: none"> has bill shape curved (up or down) has bill shape cone has bill shape conical has upperparts color brown has upperparts color iridescent has upperparts color black has upperparts color buff has upperparts color grey has upperparts color brown has head pattern brown has head pattern brown has head pattern eyebrows has head pattern striped has forehead color rufous has under tail color iridescent 	<ul style="list-style-type: none"> has under tail color purple has under tail color rufous has nape color rufous has nape color buff has wine shape tapered-wings has very long tail (32 - 72 in) has short tail-like has back pattern spotted has tail pattern striped has belly pattern solid has leg color white has wing color grey has bill color black has bill color rufous has bill color white 	<ul style="list-style-type: none"> has wing color grey has underparts color grey has throat pattern solid has head pattern crested has breast color white has throat color white has forehead color blue has forehead color white has forehead iridescent has back color white has back color grey has bill shape conical has size small (5 - 9 in) has shape toe-clinging-like has primary color white has bill color black has crown color blue has crown color black

Figure 4. Visualization of selected concepts for two examples from the CUB dataset for the best performing models in terms of clarity (Predictor-based Bernoulli) and classification performance (VLM-based ℓ_0). Green highlighting denotes concepts that are active in the ground truth. **Left:** *Cactus Wren* example with 34 ground-truth active concepts; the Bernoulli-based method selects 12 concepts, 6 of which are correct, while the ℓ_0 method selects 27 concepts, 2 of which are correct. **Right:** *Belted Kingfisher* example with 28 ground-truth active concepts; similar trends are observed, with the Bernoulli-based method selecting fewer, more precise concepts, and the ℓ_0 method selecting a larger set with lower precision.

Predictor-based ℓ_1		VLM-based Bernoulli				Predictor-based Bernoulli		VLM-based ℓ_0			
driving	driving	socializing	concrete	moist/damp	eating	driving	eating	smoke	fire	smoke	fire
biking	biking	congregating	wire	dry	socializing	congregating	foliage	electric/indoor lighting	electric/indoor lighting	electric/indoor lighting	electric/indoor lighting
hiking	natural light	waiting in line/ queuing	paper	dry	transporting	waiting in line/ queuing	foliage	gloomy	gloomy	gloomy	gloomy
camping	camping	consuming	cloth	cloud	or people	consuming	carpet	aged/ worn	aged/ worn	aged/ worn	aged/ worn
digging	digging	exercising	tree	sand	or objects	exercising	ceramic	metal	metal	metal	metal
dry	dry	playing	grass	rock/stone	or people	playing	marble	matter	matter	matter	matter
dusty	dusty	gaming	vegetation	cold	or objects	gaming	vinyl/ linoleum	rusty	rusty	rusty	rusty
vegetation	vegetation	foliage	berry	natural	or objects	foliage	in an audience	cloth	cloth	cloth	cloth
shrubbery	shrubbery	sunlight	marble	man-made	or objects	sunlight	constructing/ building	rock/stone	rock/stone	rock/stone	rock/stone
natural	natural	camping/ learning	sunlight	open area	or objects	camping	showing	ceramic	ceramic	ceramic	ceramic
foliage	foliage	being/ going/	leaves	semi-enclosed area	or objects	driving	constructing/ building	marble	marble	marble	marble
far-away horizon	far-away horizon	being in an audience	flowers	still water	or objects	driving	driving	vinyl/ linoleum	vinyl/ linoleum	vinyl/ linoleum	vinyl/ linoleum
rugged scene	rugged scene	driving	asphalt	no horizon	or objects	driving	driving	in a audience	in a audience	in a audience	in a audience
mountain	mountain	bathing	ice	no horizon	or objects	driving	driving	cloth	cloth	cloth	cloth
pavement	pavement	eating	pavement	ragged scene	or objects	driving	driving	rock/stone	rock/stone	rock/stone	rock/stone
sand	sand	medical activity	clouds	direct sun/sunny	or objects	driving	driving	ceramic	ceramic	ceramic	ceramic
dirt/soil	dirt/soil	working	brick	components	or objects	driving	driving	marble	marble	marble	marble
clouds	clouds	cleaning	matte	symmetrical	or objects	driving	driving	glass	glass	glass	glass
			cluttered space	clouds/sun	or objects	driving	driving	ocean	ocean	ocean	ocean
				direct sun/sunny	or objects	driving	driving	still water	still water	still water	still water
				components	or objects	driving	driving	clouds	clouds	clouds	clouds
				horizontal	or objects	driving	driving	symmetrical	symmetrical	symmetrical	symmetrical
				components	or objects	driving	driving	cluttered space	cluttered space	cluttered space	cluttered space

Figure 5. Visualization of selected concepts for two examples from the SUN dataset. Green highlighting denotes concepts that are active in the ground truth. **Left:** *Chaparral* example with 13 ground-truth active concepts; we choose a different set of models from the optimal in terms of clarity or accuracy, i.e., (Predictor-based ℓ_1) and classification performance (VLM-based Bernoulli). The ℓ_1 -based method selects 20 concepts, 10 of which are correct, while the Bernoulli-based method selects 54 concepts, 11 of which are correct. **Right:** *Natural History Museum* example with 5 ground-truth active concepts; here, we choose the best performing models in terms of either clarity or accuracy as before, i.e., Predictor-based Bernoulli and VLM-based ℓ_0 . The Bernoulli-based method selects fewer, more precise concepts, and finds the 5 ground truth concepts, while the ℓ_0 method selects a larger set with lower precision.